

PHOTOMETRIC STUDY OF YOUNG SOLAR ANALOGS

by  
Sean Stephen Morrison

Honors Thesis

Appalachian State University

Submitted to the Department of Physics and Astronomy  
and the Honors College  
in partial fulfillment of the requirements for Honors for the degree of

Bachelor of Science

May 2011

---

Dr. Richard O. Gray, Ph.D., Advisor

---

Dr. Dale E. Wheeler, Ph.D., Second Reader

---

Dr. Richard O. Gray, Ph.D., Physics and Astronomy  
Departmental Honors Director

---

Dr. Leslie Sargent Jones, Ph.D., Director, The Honors  
College

Copyright © 2011 Sean Stephen Morrison

All Rights Reserved

## ABSTRACT

### PHOTOMETRIC STUDY OF YOUNG SOLAR ANALOGS

May 2011

Sean Stephen Morrison

This thesis discusses solar type stars that are between 0.3 and 1.5 Gyr old, otherwise known as young solar analogs (YSAs). It explores how they are defined, the methods used to study them, and the state of research in the field. The study of young solar analogs offers us a window into the conditions in the early solar system when life was establishing a foothold on the Earth. The theories of the young Sun predict that early life had to contend with a hostile space environment; strong ultraviolet fluxes without the benefit of a protective ozone layer; enhanced solar winds, flares and magnetic storms, perhaps strong enough to compromise temporarily the earth's magnetosphere; and a variability in the solar constant at least an order of magnitude greater than what the Earth experiences today. This research strives to determine how accurate these theories are by studying stars that have the same dynamics as the Sun did during the early solar system. This paper also gives a detailed description of the techniques, instruments, and setups that I have used in my preliminary photometric study of YSAs at Appalachian State University. It also gives a summary of our preliminary results and conclusions from the data that we have obtained over the course of this project.

## ACKNOWLEDGMENTS

I would like to acknowledge Dr. Richard O. Gray, without whose guidance, support, and encouragement, this project would not have been possible.

I also wish to thank Dr. Jon M. Saken for his help in setting up the robotic telescope, and Michael D. Hughes for his help in debugging the robotic mount when it malfunctioned.

I would also like to acknowledge the North Carolina Space Grant and Appalachian State University's Office of Student Research for their grants for research and equipment, which helped make the research possible.

Finally, I would like to thank my family, friends, and especially my girl friend, Mandy Shoaf, for the support and understanding they have all shown.

# Contents

<b>Table of Contents</b>	<b>v</b>
<b>List of Figures</b>	<b>vii</b>
<b>1 Introduction</b>	<b>1</b>
1.1 Theoretical Background . . . . .	2
1.1.1 Stellar Structure and Sunspot Physics . . . . .	3
1.1.2 Ca II K & H Fluxes . . . . .	4
1.1.3 Additional Fluxes . . . . .	5
1.2 Early Research . . . . .	5
1.2.1 Ca II K & H Monitoring at Mount Wilson Observatory . . . . .	5
1.2.2 “Sun in Time” . . . . .	8
1.3 Current Research . . . . .	9
1.3.1 Lowell Observatory Solar-Stellar Spectrograph . . . . .	9
1.4 YSA Spectroscopic Research at Appalachian State University . . . . .	11
1.4.1 Spectroscopic Result . . . . .	11
1.4.2 Future Developments . . . . .	11
<b>2 Selection of the YSA Stars for Study</b>	<b>14</b>
<b>3 Photometric Observations</b>	<b>17</b>
3.1 PROMPT Array and Skynet . . . . .	17
3.2 Piggyback Telescope on the DSO 0.8-m . . . . .	18
3.2.1 5-inch (0.127-m) f/10 Celestron . . . . .	18
3.2.2 6-inch (0.1524-m) Wide-field f/9 Ritchey-Chrétien . . . . .	19
3.3 The Automated Photometric Telescope on a Robotic Mount . . . . .	21
3.3.1 Telescope Attributes . . . . .	21
3.3.2 Mount . . . . .	22
3.3.3 Automation . . . . .	25
3.3.4 Future Changes . . . . .	26
<b>4 Flat-Field Experiment</b>	<b>27</b>

---

<b>5</b>	<b>Reduction and Photometry Pipeline</b>	<b>31</b>
<b>6</b>	<b>Results</b>	<b>33</b>
6.1	HD 189733 . . . . .	33
6.1.1	Multiple Comparison Star Test . . . . .	35
6.2	HD 209393 . . . . .	37
<b>7</b>	<b>Conclusions</b>	<b>42</b>
<b>A</b>	<b>IRAF imageproc_final.cl code</b>	<b>46</b>
<b>B</b>	<b>IRAF photometry.cl code</b>	<b>54</b>

# List of Figures

1.1	Mount Wilson Observatory Results . . . . .	7
1.2	Times Series of Ca II K & H observations . . . . .	12
1.3	HD 82885 Flare . . . . .	13
3.1	DSO 5-inch Piggyback . . . . .	19
3.2	DSO 6-inch Piggyback . . . . .	20
3.3	Orion Telescope on Robotic Mount . . . . .	22
3.4	Wide-field f/9 Ritchey-Chrétien on Robotic Mount . . . . .	23
4.1	Residual in I . . . . .	28
4.2	Residual in V . . . . .	29
4.3	Residual in B . . . . .	30
6.1	HD189733 Light Curves . . . . .	34
6.2	HD189733 Finder Chart . . . . .	34
6.3	The Effect of Clouds . . . . .	36
6.4	The Effect of Drift . . . . .	37
6.5	The Effect of Focus . . . . .	38
6.6	HD209393 Light Curves . . . . .	40
6.7	HD209393 Finder Chart . . . . .	41

# List of Tables

2.1	This table includes the list of the objects that are the targets of interest for the YSA Spectroscopic and Photometric Research at Appalachian State University along with stellar characteristics of interest to both projects. The “(k)” in the spectral type “(SpT)” column designates if the spectra has visible emission reversals. . . . .	16
6.1	This table includes the results of the multiple comparison star test on HD 189733. In this table, star 1 is HD 189733 and stars 2, 3, and 4 are the comparison stars. . . . .	39

# Chapter 1

## Introduction

Indirect evidence of what the Sun was like during its youth can be seen through fossil and mineral records, while direct evidence is not obtainable from any source in our solar system. Direct evidence is only obtainable by looking at stars that are similar in properties to the early Sun, i.e. young solar analogs (YSA), with ages between 0.3 and 1.5 Gyr. The study of YSAs offers us a window into the conditions in the early solar system when life was establishing a foothold on the Earth. These studies, done both photometrically and spectroscopically, are long-term and ongoing.

The conditions of the space environment, including solar radiation, the solar wind, and solar storms, affect the modern Earth. The current theories, as stated in Gaidos et al. (2001), suggest that in the early solar system when the Sun was more active, and there was more orbital debris left over from the formation of the solar system, the Earth and other planets were affected more severely than in the modern solar system. Gaidos et al. also state that models for the early Sun predict a solar luminosity between 70% and 75% of the current solar luminosity. This means that if all else were equal, the temperature of the Earth would have been below freezing, which

would not be conducive for the formation of life on Earth.

The Young Solar Analogs Project studies stars with spectral types ranging from late F- to early K-type. The Sun currently falls in this range with the spectral type of G2, and also did when it was on the Zero-Age Main Sequence as a  $\sim$ G5. Although cooler and less massive stars have longer main-sequence lives, and thus more time for life to develop, the habitable zone would be so close-in to the star that planets in that zone would be tidal locked leaving one side exposed to the Sun at all times, while the other side would never receive light. This would lead to very un-Earth-like conditions on such a planet.

Stellar activity is most often characterized as the dynamics of the magnetic field of the star. The magnetic field causes starspots, flares, and coronal mass ejections, which affect the temperature, climate, and atmosphere on the planets orbiting the star.

## 1.1 Theoretical Background

Stellar spectroscopy, along with laboratory experiments, have shown that stars emit across the electromagnetic spectrum. Stellar spectra show both absorption and emission lines corresponding to energy transitions in neutral atoms, molecules and ions in different atmospheric layers. This creates the spectrum of the star. The spectrum can be used to characterize the star. Fluxes in the far-ultraviolet (FUV), extreme-ultraviolet (EUV), and X-ray in solar type stars arise from plasmas heated to very high temperatures ( $T > 50,000\text{K}$ ) and are indicators of strong local enhancements in the stellar magnetic field. These fluxes are difficult to monitor continuously since they require space-based telescopes, and so proxies such as the Ca II K-line at 3933.7

$\text{\AA}$  and the Ca II H-line at  $3968.5 \text{ \AA}$  are observed. The cores of these spectral lines are formed in the chromosphere of the star, and long-term studies (Baliunas et al., 1995) have shown that the Ca II K & H chromospheric fluxes are well correlated with sunspots and other magnetic activity on the Sun. The spectrum of a star can give a wealth of information about the star.

### 1.1.1 Stellar Structure and Sunspot Physics

The atmospheres of the Sun and other stars are composed of a number of different layers. These layers include the photosphere, the chromosphere, and the corona. The photosphere is the layer of the star that is visible in white light. This layer, which has a thickness that is only a small fraction of the stellar radius, generates most of the light emitted from the star. This is the layer where the sun spots are present. The next layer out is the chromosphere and beyond that is the corona. Solar flares extend from the photosphere out to the corona.

Sunspots are areas of cooler temperature on the Sun's surface that appear dark as a result, even though they are actually quite bright. Sunspots are regions of strong magnetic fields in the photosphere that inhibit convection and thus heat flow to the surface. The standard framework for understanding sunspots and the sunspot cycle is the Babcock Model. This model suggests that sunspots are formed from a progressive tangling of the solar magnetic fields. As magnetic fields in the Sun are "frozen" into ionized gas, and the gas is sheared through the differential rotation of the Sun, the magnetic field lines are twisted and tangled around the Sun. This process causes the formation of sunspots and is cyclical. In the Sun, that cycle lasts about 11 years.

In addition to sunspots, there is another phenomenon known as faculae, that is a direct result of clusters of magnetic field lines. These differ from sunspots in the

fact that instead of being darker than the surrounding surface of the Sun, they are brighter. During periods of maximum solar activity and maximum sunspots, the Sun is actually brighter than at other times because of the presence of faculae.

When areas of opposing magnetic fields meet, they cancel each other out in an event that astronomers call magnetic reconnection. When this happens energy is released and flares occur. A flare occurs when energy stored in the magnetic fields is released in the form of short-wavelength photons and high-energy protons and electrons.

The magnetic field of the Sun, through a process called magnetic heating, heats the upper levels of the atmosphere of the Sun (i.e. the chromosphere and the corona) and keeps them at their characteristic temperatures.

As the Sun and other stars age, their rotation rate and activity levels change. A younger star has a higher rotation rate than older stars. This slowing of the rotation rate as a star ages is a result of the loss of energy and angular momentum via the solar wind and radiation. This decrease in rotation rate is associated with a decrease in stellar-activity levels. It can be argued that if the Babcock Model is accurate, then as the rotation slows, magnetic-field entanglement is reduced, thus reducing activity levels.

### **1.1.2 Ca II K & H Fluxes**

The Ca II K-line at 3933.7 Å and the Ca II H-line at 3968.5 Å convey information about conditions in the chromosphere. The cores of these lines are formed in the stellar chromosphere. Recent studies have shown that Ca II K & H fluxes are well-correlated in solar-type stars with both X-ray luminosities (Hempelmann (2003); Favata et al. (2004)), and FUV excesses. Areas of concentrated magnetic fields in the

chromosphere of the Sun form these lines much more intensely than areas with weaker magnetic fields. They are a result of non-thermal heating in the chromosphere, i.e. heating produced by local differences in the magnetic field and magnetic reconnection. Baliunas et al. (1995) state that because of this, these fluxes are a useful spectroscopic indicator of the strength and area of strong magnetic fields and thus starspots.

### **1.1.3 Additional Fluxes**

To obtain a full picture of stellar activity, it is necessary to observe and if possible monitor over long time periods, not only the Ca II K & H fluxes, but also fluxes in the X-ray, EUV and FUV. This is important because these shorter wavelengths sample not only the chromosphere, but also the coronal and transition regions.

## **1.2 Early Research**

Over the years, a number of studies and monitoring projects have been conducted on solar analogs. These studies included a long-term monitoring of such stars at the Mount Wilson Observatory.

### **1.2.1 Ca II K & H Monitoring at Mount Wilson Observatory**

Long term monitoring of Ca II K & H fluxes began at Mount Wilson Observatory in 1966 according to Baliunas et al. (1995); Wilson (1978). This project was completed in 2003 after 37 years of near continuous spectroscopic monitoring of a hundred stars with spectral types ranging from mid-F to M2.

These stars, in addition to having spectral types from mid-F to M2, also ranged from young stars with very active chromospheres to old stars with minimal activity.

Of the 100 stars in the sample, only about 15 fit our definition of YSAs. In about 60% of the sample, stellar activity cycles similar to that of the Sun were discovered. Furthermore, in about 25% of the sample, there were no well-defined cycles. The remaining 15% of the sample showed little to no variations in activity.

This Mount Wilson Observatory project defined and used an “activity index”,  $S$ , that can be calculated from observations through a number of different wavelength bands. This quantity,  $S$ , is defined to be

$$S = \alpha \frac{H + K}{V + R}, \quad (1.1)$$

where  $H$  and  $K$  are fluxes in the 1 Å wide bands centered on the CaII K & H lines respectively, and  $V$  and  $R$  are fluxes in continuum bands situated short-wards and long-wards of the Ca II lines respectively.  $\alpha$  is a calibration constant that was determined nightly based on the conditions. The  $S$  value is assumed to be a good indicator of chromospheric activity related to the strength of the magnetic activity of a star.

The color of a star can be determined by brightness measurements through a standard B (blue) and V (green) filters. The B-V color index is then formed from the difference of the B and V magnitudes. The Mount Wilson project found a relationship between the S-index and the (B-V) color as shown in Figure 1.1. The Mount Wilson researchers found that the S-index is sensitive to the stellar photospheric temperature, causing  $\langle S \rangle$  to increase as (B-V) increases. For example, orange-red stars in their sample of spectral type K, with low  $\langle S \rangle$  values have pronounced activity cycles, while white or yellowish-white stars, of spectral type F, with low  $\langle S \rangle$  values have nearly constant or slow variations. These F-type stars have shallow convection zones with rapid rotation compared to the Sun, which tends to produce activity cycles that are very different than the Sun according to Baliunas et al. (1995).

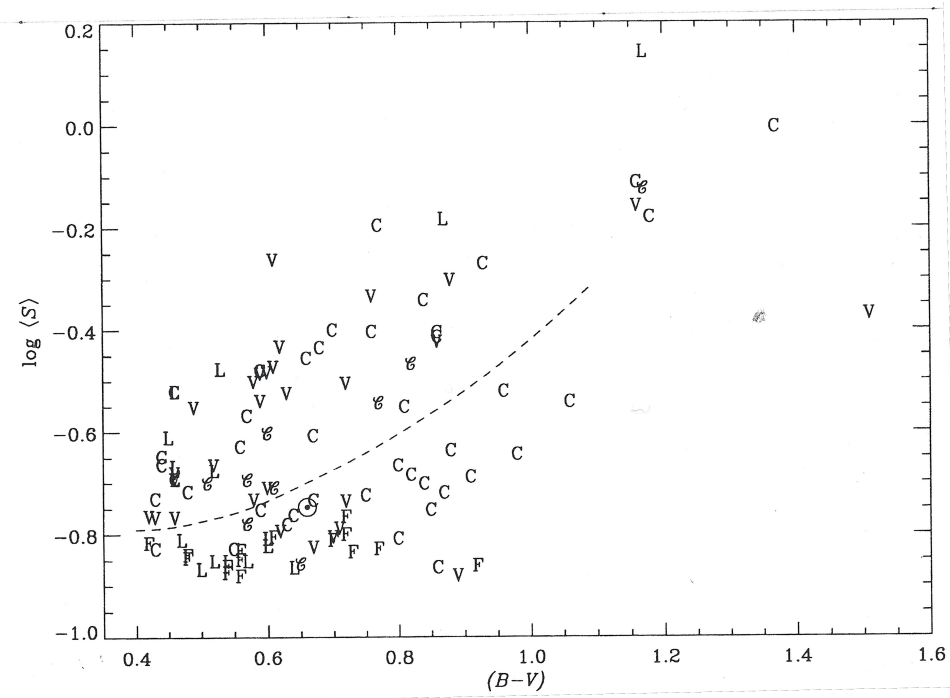


**Figure 1.1** The distribution of chromospheric activity with B-V (roughly equivalent to mass in lower main-sequence stars) along with long term variability classification. Stars with ‘C’ classifications have measured activity cycle periods; those labeled ‘℄’ have secondary periods. Stars labeled ‘V’ have variable activity with no clear period; ‘L’ means long-term trends; ‘F’ means flat with little or no change in activity. The position of the Sun (⊙) is also marked. The dashed line roughly separates the stars with high or low  $\langle S \rangle$ . (Baliunas et al., 1995)

Baliunas et al. (1995) points out that in yellowish stars of spectral type G such as the Sun, only stars with low  $\langle S \rangle$  values have very low chromospheric variations and activity levels. These episodes of low activity and variability might be similar to the episodes of low magnetism such as the prolonged sunspot minimum, such as the Maunder Minimum of the seventeenth century.

On the contrary, stars with “flat” records generally have slow rotations and are therefore old. This suggests that the Maunder Minimum phase appears only in old stars. However, age may not be the only explanation for the Maunder Minimum since not all stars fit that trend. Some young stars also show this minimum, while other old stars do not, which could suggest that the Maunder Minimum is actually just a temporary stage in stellar evolution.

It was found that none of the stars in the sample have activity cycles with periods less than 7 years. The Mount Wilson results also found that stellar variability, at least within the studied sample, is richer than that of the Sun.

### 1.2.2 “Sun in Time”

The “Sun in Time” (Guinan & Engle, 2009) project was established in 1988 to study starspots and luminosity variations of solar-type stars of different ages. It was designed to carry out a multi-wavelength study of a sample of solar analogs over the course of 20 years.

The “Sun in Time” project sampled solar analogs of spectral types G0 to G5. A solar analogue is a star that roughly approximates the mass and spectral type of the Sun, what astronomers would identify as a main-sequence dwarf between spectral types G0 and G5 (the solar spectral type is G2). The ages of the stars ranged from 50 Myr to 9 Gyr. Of the stars in the sample, only 4 or 5 were within the YSA parameters

of 0.3 to 1.5 Gyr.

This project found evidence that the early Sun was rotating 10 times faster than at present. The early Sun is also modeled as having coronal X-ray and transition-region/chromospheric EUV and FUV fluxes several hundred times higher than the present. It also helped to confirm that the Ca II K & H observations are useful proxies for estimating X-ray, EUV, and FUV fluxes and variability. The program also refined the rotation-age-activity relationship of Soderblom (1982, 1983) for solar-type stars.

## 1.3 Current Research

There are a number of ongoing projects studying solar analogs. These studies cover both spectroscopic and photometric fluxes. The photometry covers a variety of spectral bands from the blue to the infrared.

### 1.3.1 Lowell Observatory Solar-Stellar Spectrograph

The Lowell Observatory Solar-Stellar Spectrograph (SSS) program started in 1988 and is ongoing. It is a project dedicated to long-term observations of the Sun and Sun-like stars (Hall et al., 2009). It uses a different approach from the earlier projects. This approach is a direct comparison between the Sun and solar analogs. This is carried out through the use of a fiberoptic-fed spectrograph which allows the observation of both the Sun and faint stars with the same instrument. This allows direct comparison of the Sun's variations to those of its cousins. The dynamics of the sample also differ greatly from that of the Mount Wilson program. The SSS offers not only broader spectral coverage than the Mount Wilson photometer, but also the opportunity to observe both the Sun and the stars with the same spectrograph via dual fiber feeds.

Other programs have typically required indirect observations (e.g., of the Moon) to obtain “solar” measurements.

At this time, the Lowell Observatory SSS sample consists of 28 stars of which only 6 are YSAs. These stars have spectral types that range from F8 to G8, with most in the range of G0 to G2, which are similar to the Sun’s spectral type, which is currently a G2V. Many of these stars are “solar twins.” This means that they have ages and metallicities almost identical to that of the current Sun, as opposed to “YSAs” which have activity levels much higher than the Sun, but are similar to the Sun at a young age.

Lowell Observatory, unlike the Mount Wilson project, carries out high-precision photometric observations nearly simultaneously with the spectroscopy. The photometric observations are carried out in the Strömgren b and y bands, at 4662 Å and 5456 Å, respectively according to Lockwood et al. (2007). These joint observations led to some interesting results.

Some of the stars in the SSS sample act similarly to the Sun and were brightest during periods of highest activity. Others act contrary to what might be expected and showed the lowest luminosities when they were most active. In general, most of the active stars in the sample, i.e. the YSAs, showed an inverse correlation between brightness and activity, while most of the “solar twins” showed a direct correlation between brightness and activity. These data suggest that stars, as they age and decline in activity, flip from an inverse to a direct correlation between activity and brightness. The results of the program are limited because the sample has a limited spectral range of G0 to G2. Nor does this project give a full picture of stellar activity at the early epoch of 0.3 Gyr to 1.5 Gry.

## **1.4 YSA Spectroscopic Research at Appalachian State University**

In 2007, Dr. Richard Gray started a pilot project of monitoring  $\sim 40$  stars at Ca II K & H using the 0.8 m telescope and spectrograph at Appalachian State University's Dark Sky Observatory (DSO). In particular, Dr. Gray was looking at the cores of these lines which give a large amount of information about the magnetic fields in the chromosphere and corona.

### **1.4.1 Spectroscopic Result**

Over four observing seasons, spectroscopic measurements have been taken to determine the rotational periods and activity levels for a number of the stars in the sample using the Ca II K & H measurements as shown in Figure 1.2. In addition, the record now appears to be long enough that long-term variations in stellar activity levels have begun to appear (see Figure 1.2). Flare events in YSAs can also be observed spectroscopically (see Figure 1.3).

### **1.4.2 Future Developments**

Dr. Gray plans to continue the YSA project as a full-fledged program. He also plans to expand his spectroscopic work using the Vatican Advanced Technology Telescope (VATT) and its recently commissioned stellar spectrograph (VATTspec). The shorter exposure times permitted by the VATTspec will allow for more observations and detection of short-term changes in stellar activity. The VATTspec and the VATT telescope are needed for the high-resolution spectra required to get the most data from every observation. Dr. Gray's colleague at the VATT is Chris Corbally, the

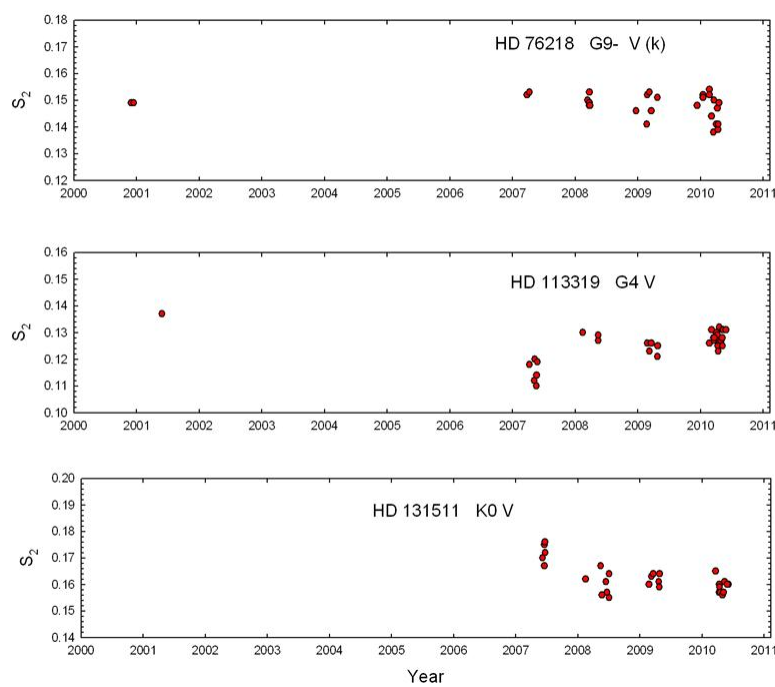


**Figure 1.2** Time series of Ca II K & H observations for HD 76218, HD 113319, and HD 131511. Each of these series shows activity variations during the four observing seasons of the pilot project.

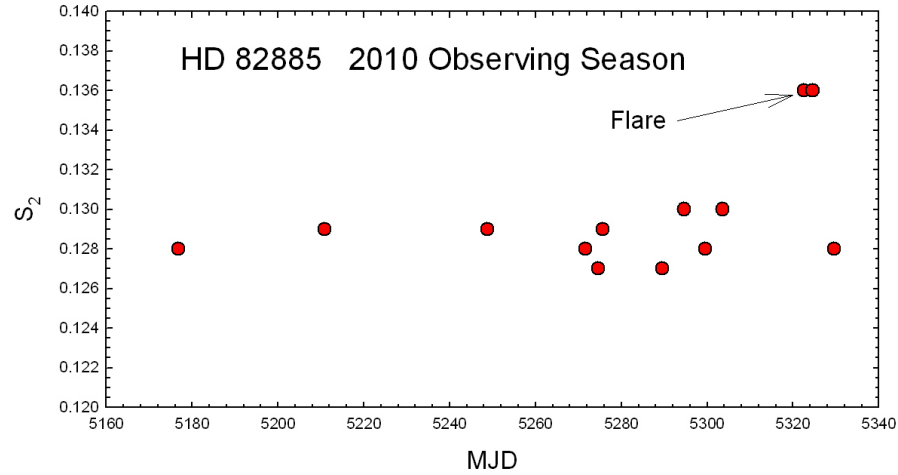


**Figure 1.3** A probable flare event observed in the star HD 82885 during the 2010 observing season. The event lasted at least two consecutive nights.

vice director of the Vatican Observatory, and this will allow for extensive allocation of time to this project. Dr. Gray hopes to send students to use the VATT, but at the very least, he and his students will be able to control the VATT remotely in the future.

## Chapter 2

# Selection of the YSA Stars for Study

The stars studied in this thesis are based on a sample of YSAs carefully selected from the Nearby Stars Project, which was a spectroscopic survey of stars earlier than M0 within 40 parsecs of the Earth. The YSA sample was later narrowed to 31 high priority stars, with the others reduced to secondary targets through a combination of experimental analysis and modeling (see Table 2.1). The sample consists of stars with spectral types ranging from F8 to K2 with ages between 0.3 and 1.5 Gyr. All of the stars have V magnitudes in the range from 8 to 5 and are main-sequence (unevolved dwarfs) that are in single-star systems or in wide visual-binary systems.

This sample is the same as used by Dr. Richard Gray and his colleagues in their spectroscopic study of young solar analogs. At the completion of both studies, these results will be combined to give a full and complete understanding of what is happening with each of the stars. This collaboration also includes the use of a piggyback telescope on the spectroscopic telescope so that one observer can obtain

both photometric and spectroscopic data during a single night.

The brightness of these stars allows for short-length exposures of each star. This is a major advantage to both Dr. Gray's spectroscopic study and this photometric study because it allows an observer to image the largest number of objects possible on any given night. It also allows for a small aperture photometric telescope which decreases the cost of a long-term monitoring project.

YSA Sample and Stellar Characteristics

Name	SpT	V	Age (Gyr)	Name	SpT	V	Age (Gyr)
HD 5996	G9 V (k)	7.67	0.5	HD 124694	F8 V	7.19	0.6
HD 9472	G2+ V	7.64	0.4	HD 130322	G8.5 V	8.04	1.2
HD 13531	G7 V	7.35	0.3	HD 131511	K0 V	6.01	0.3
HD 27685	G4 V	7.84	0.7	HD 138763	F9 V	6.53	0.3
HD 27808	F8 V	7.12	0.7	HD 149661	K0 V	5.76	1.4
HD 27836	G0 V (k)	7.60	0.7	HD 152391	G8.5 V (k)	6.64	0.7
HD 27859	G0 V (k)	7.80	0.7	HD 154417	F9 V	6.01	0.5
HD 28394	F8 V	7.02	0.7	HD 170778	G0- V (k)	7.50	0.3
HD 42807	G5 V	6.44	0.3	HD 189733	K2 V (k)	7.68	0.5
HD 76218	G9- V (k)	7.69	0.5	HD 190771	G2 V	6.17	0.7
HD 82885	G8+ V	5.41	1.6	HD 192263	K2 V (k)	7.79	1.0
HD 96064A	G8+ V (k)	7.64	0.3	HD 206860	G0 V	6.00	0.4
HD 101501	G8 V	5.32	1.4	HD 209393	G5 V (k)	7.96	0.5
HD 102195	G9.5 V (k)	8.06	1.1	HD 217813	G1 V	6.66	0.7
HD 113319	G4 V	7.52	1.5	HD 222143	G3 V (k)	6.58	0.8
HD 117378	F9.5 V	7.64	0.5				

**Table 2.1** This table includes the list of the objects that are the targets of interest for the YSA Spectroscopic and Photometric Research at Appalachian State University along with stellar characteristics of interest to both projects. The “(k)” in the spectral type “(SpT)” column designates if the spectrum has visible emission reversals.

# Chapter 3

## Photometric Observations

Observations have been carried out on a number of different instruments during the development of the project. All of the telescopes are considered small aperture telescopes with the largest being the 0.41-m telescopes of the PROMPT array.

### 3.1 PROMPT Array and Skynet

I started this project in Fall 2009 using the automatic photometric telescopes of the Skynet/PROMPT project (Reichart et al., 2006). The PROMPT telescopes are five 0.41-m Ritchey-Chrétien telescopes. Each telescope in the array is remotely controlled by the Skynet system. This system allows for prioritized queue-driven observing by observers all over the world. While this system is convenient, it does not allow an individual observer to take his or her own calibration images, but instead takes standard images at the start of every night. This limitation in the calibration images causes a limitation in precision that forced us to stop using the system. These limitations are primarily a result of the flat fields. We think that the open truss design and the clam shell dome of the PROMPT telescopes caused the calibration

images to exhibit gradients and abnormalities that limit the usefulness of the these images.

## 3.2 Piggyback Telescope on the DSO 0.8-m

The piggyback telescope on Appalachian State's Dark Sky Observatory's 0.8-m spectroscopic telescope, which replaced the PROMPT array as our instrument of choice in the fall of 2010, has taken on two different forms throughout its short life time. This telescope allows for simultaneous spectroscopic and photometric observing for the Young Solar Analog Project. While this limits the number of stars that the project can monitor photometrically in a single night, it also allows for a better understanding of the behavior of the program stars.

### 3.2.1 5-inch (0.127-m) f/10 Celestron

The first telescope that was mounted as a piggyback telescope was a 5-inch (0.127-m) f/10 Celestron telescope. It was equipped with a SBIG ST-402ME CCD imager with built-in filter wheel. The filter wheel is equipped with Johnson-Cousins B, V, and I filters, as well as a clear filter. While this setup was sufficient, it only had a 15 by 20 arc minute field of view, which limits the number of comparison stars in the field. The calibration flat fields are provided by a luminescent flip-flat panel. In addition, this flip-flat also acts as a telescope lens cap keeping the optical surfaces covered when not in use. This telescope and setup is shown in Figure 3.1.

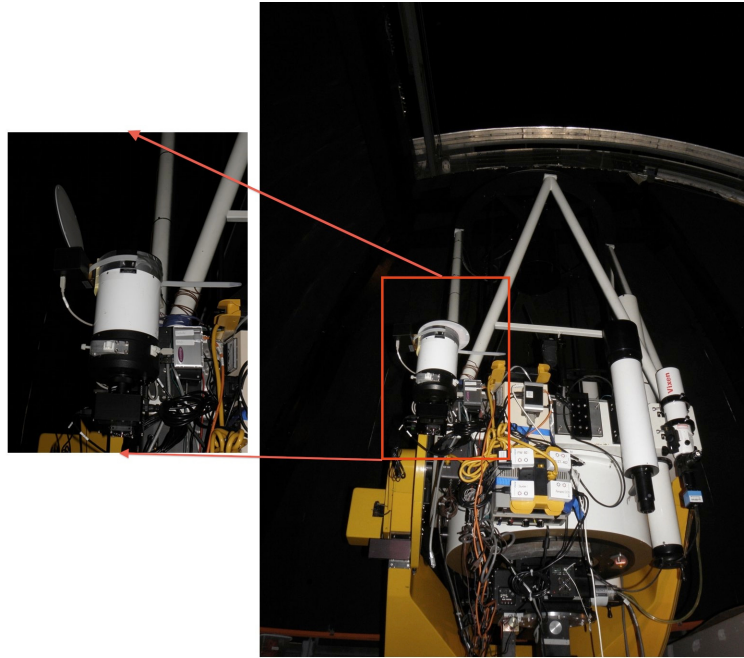


**Figure 3.1** DSO 0.8-m telescope with 5-inch piggyback telescope shown in inset.

### 3.2.2 6-inch (0.1524-m) Wide-field f/9 Ritchey-Chrétien

The 5-inch telescope was replaced by a 6-inch (0.1524-m) wide-field f/9 Ritchey-Chrétien telescope. The old CCD was replaced with a “large format” SBIG ST-8300 CCD. The combination of these two improvements increased the field of view by three to four times, giving a new field of view of nearly one degree. This allows for an improvement in the precision of the photometry because of a greater number of comparison stars. The same calibration flat-field method used for the original telescope is also used for this one. The new CCD’s filter wheel is equipped with Johnson-Cousins B, V, and R, along with a hydrogen-alpha filter and a Strömgren v filter. It is equipped with the same luminescent flip-flat panel as the first telescope, which as before, also acts as a telescope lens cap. This telescope and setup is shown in Figure 3.2.

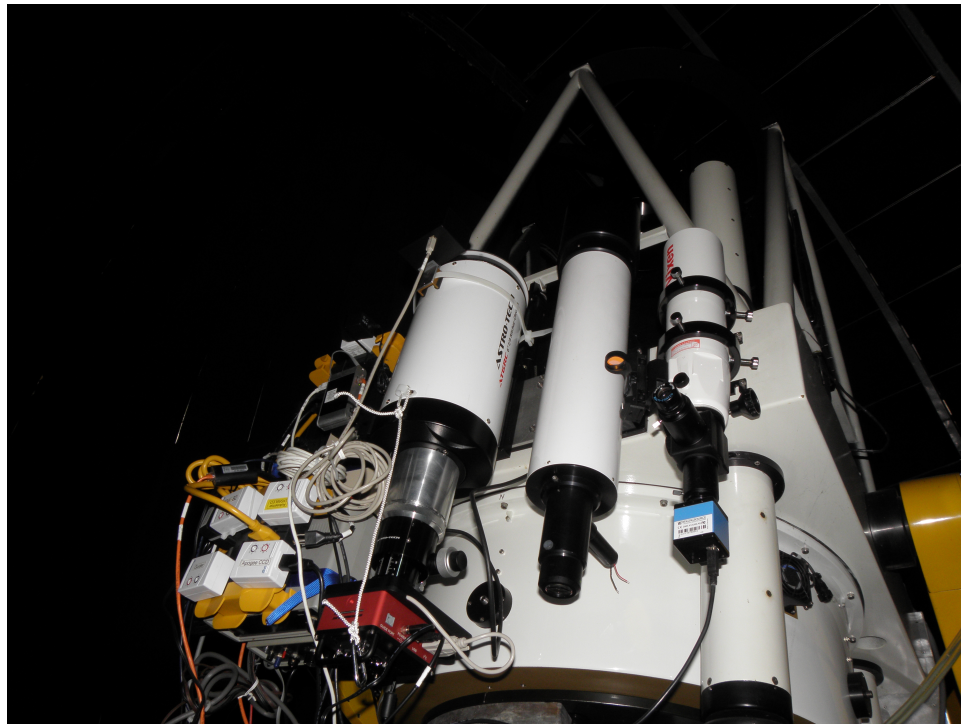


**Figure 3.2** DSO 0.8-m telescope with the new 6-inch wide-field f/9 Ritchey-Chrétien piggyback telescope shown as the left-most piggybacked telescope.

## 3.3 The Automated Photometric Telescope on a Robotic Mount

In addition to the piggyback scope, this project called for the development of an automated photometric telescope on a robotic mount. This was required because it will allow for more continuous monitoring of the stars than allowed by time constraints on the shared DSO 0.8-m. The DSO 0.8-m is only allocated for use by Dr. Gray for his spectroscopic projects and this project for about one-third of the nights in any given month. Also, since spectroscopy requires longer exposures, it sits on a star for much longer than is required for photometric measurements. The robotic telescope allows for the observation of every visible program star on any given night since it is only taking photometry, which requires shorter exposure times than spectroscopy. This telescope will eventually be placed in a housing of its own at Appalachian State's Dark Sky observatory. Once there, the minimal human control that is required will be done via remote internet connection from campus or elsewhere.

### 3.3.1 Telescope Attributes

The robotic mount, over its short lifespan, has carried two different telescopes. The first telescope was a Orion Apex 102mm Maksutov-Cassegrain Telescope with an f/12.7 focal ratio. It was equipped with a SBIG ST-402ME CCD imager with built-in filter wheel. The filter wheel had the Johnson-Cousins B, V, and I filters, as well as a clear filter. The telescope that replaced the first is an identical telescope and CCD to the second piggyback telescope. It is also equipped with the same style of luminescent flip-flat panel. This is convenient, because it allows us to keep the optical surfaces covered when not in use while allowing the observer to open it remotely. The first



**Figure 3.3** The original Orion telescope on the robotic mount, shown without the cord wrap prevention rod mounted.

telescope is shown in Figure 3.3, while the replacement is shown in Figure 3.4.

### 3.3.2 Mount

The mount used is an iOptron MiniTowerPro. This commercially available mount is an AltAz mount. It uses the iOptron GoToNova 8401 controller in standard operation, but the controller has a USB port that allows for computer control via ASCOM drivers. The mount also includes a GPS which allows for precise stellar alignment. It uses a dovetail mount to mount the primary telescope and has the option to mount either a second telescope or counterweight on the opposite side. The latest firmware updates have included an innovative option that limits the mount motion to prevent cord wrap, which we utilize to allow for unmonitored observing.



**Figure 3.4** The replacement wide-field f/9 Ritchey-Chrétien telescope on the robotic mount, shown with the cord wrap prevention rod mounted in its temporary housing at the Rankin Science Observatory.

### Issues

During the process of setting up the mount, a number of issues were encountered. When the telescope mount was initially connected to the computer using the default drivers, a number of problems ensued. When I tried to slew the telescope using the software built into TheSky6, the program would give an error for the first slew. This did not seem to be a major issue at first until I tried to slew it again, which caused the program to lockup and crash. This is a major issue because if the mount control software does not work with the drivers, then automation is impossible. We then tried to connect the mount to MaxIm DL 5 to use its observatory control tools, but it would not even connect nor would other similar software that we tried. As a result, we communicated with the company to have the issues resolved. After no luck determining a solution with the company, I turned to various online forums to look for help. I was told by various people that I had two different options. These were to

update to TheSkyX or to try using the Vixen Sky Sensor 2000 driver. Since the latter was free, we tried using the alternate driver and had success. We also discovered later that the standard drivers do not work with MaxIm DL, which is an issue known by the company.

On the first night testing the setup with the new driver, I noticed that even when tracking was engaged, stars were drifting across the field of view of the CCD. To remedy this, I attempted to re-sync a star. While doing this, the hand-control paddle froze up and I was forced to restart it. Upon restart, the controller came up saying “Warning! Can not communicate with DEC motor controller.” After some diagnostics with the help on the tech support staff at iOptron and Appalachian’s Electronics Technician, we determined that it was a fault on the circuit board. I passed this along to the technical support, who agreed to send us a new circuit board along with a new hand-control paddle. When these arrived, I first tried swapping out the circuit board, but that did not fix the issue. I then swapped out the hand controller leaving the new circuit board in place. This fixed the error which allowed me to continue testing of the mount.

We also initially had to deal with the cord wrap issues associated with an Alt-Az mount. To try and solve this we mounted a piece of piping to the top of the mount and ran the wires up that pipe and to the computer from there. We also mounted a USB-to-ethernet-to-USB extender. This allowed us to only have two cables, power and ethernet, running to the mount. This was ideal since ethernet cables are more durable than USB and thus, would be less likely to be damaged with cord wrap. We had used this same USB extender on the piggyback telescope at DSO, which is where we determined the flaw in this setup. At DSO, it was discovered that this USB extender does not work in temperatures much below room temperature. At this

point, we were unsure with what to replace the unit. Then, while working to try and diagnose the circuit board issue discussed above, I came across a setting in the newest driver release that limits the mount's Azimuth motor from going more than 360 degrees. This setting eliminated the need for the USB-to-ethernet extender since cord wrap was no longer an issue, which in turn allowed us to use standard USB extended-length cords. This setup also allowed me to remove the piping rig from the top of the mount and run the cables directly.

### 3.3.3 Automation

The automation of the mount and camera uses Appalachian State observatory's standard observing software suites of TheSky6 and MaxIm DL 5. These two programs are controlled by another program called CCD AutoPilot4. CCD AutoPilot4 does continuous pointing corrections to eliminate tracking errors. It allows the user to input a list of objects and exposures at the start of the night and have all the observing done without any more input from the user. In addition, the software collects dark and bias frames throughout the night and carries out automatic sky flats at dusk and dawn. One convenient feature that it has is the ability to control the flip-flat, thus making it ideal for our setup.

Once the mount and telescope are placed in their final position at the Dark Sky Observatory, this software will allow for minimal daily intervention by a researcher. All the researcher will be required to do is upload a list of objects to be observed during the night and then set the exposure times for each object. From that point on, CCD AutoPilot4 takes over and controls the movement of the mount along with the different exposures. When it comes time to take the flat fields, the software moves the flip-flat into position and illuminates the panel to the set level for each individual

filter and then takes the flat.

### **3.3.4 Future Changes**

In the future, this telescope and mount will be moved from its temporary housing at the Rankin Science Observatory's Introductory Roll-off Roof Lab and its temporary storage location at the Dark Sky Observatory, and placed in a permanent housing of its own, either in the form of a roll-off roof structure or new dome at the Dark Sky Observatory. It might also, depending on whether need is shown for it, have dew heaters installed on the front end of the telescope and possibly on the flip-flat.

# Chapter 4

## Flat-Field Experiment

Most astronomers use sky flats to calibrate photometric images, but our telescopes use a completely different method that employs a luminescent panel called a “Flip-Flat”. A sky flat is an image taken at either dusk or dawn in an area of the sky that does not have bright stars in the field. This image is then used to eliminate the optical effects caused by dust and abnormalities in the optical surfaces and CCD.

To validate the “Flip-Flat” method, we took flat fields using both the standard method and the “Flip-Flat” for each filter. For each method and each filter, a master flat was created. Master flats are created by first subtracting darks from the images. These images are then combined and normalized to unity. The set of flip-flat flats were divided by their corresponding sky flat. These residuals were then normalized to unity and examined.

These residuals are illustrated with the I-band residual shown in Figure 4.1, the V-band residual in Figure 4.2, and the B-band residual in Figure 4.3. Each of these residuals show only minute systematic differences, which amount to much less than a 1% residual between the two different types of flats. Due to this difference of less

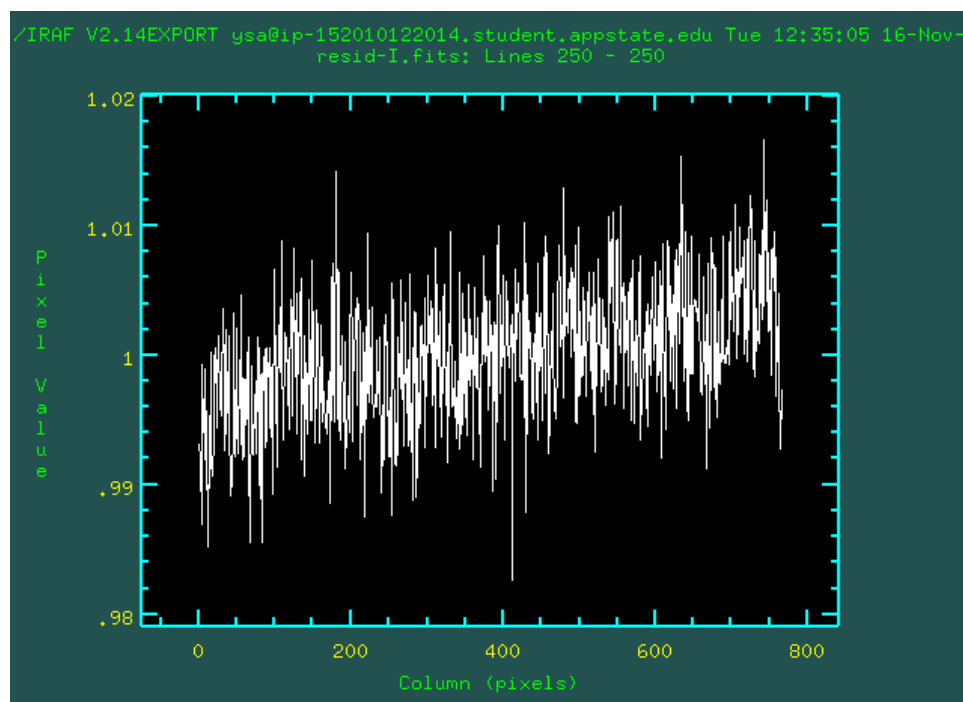


**Figure 4.1** Horizontal slice of the residual of the I-filter flat fields showing a difference of  $\sim 0.5\%$  across the chip.

than 1%, there is significant evidence that the flip-flat is a viable method for obtaining flats. This is important because the flip-flat allows flats to be taken at any point of the day or night, which gives much more flexibility in an observing run. It also allows for flats to be taken in the middle of the observing run if the need arises.

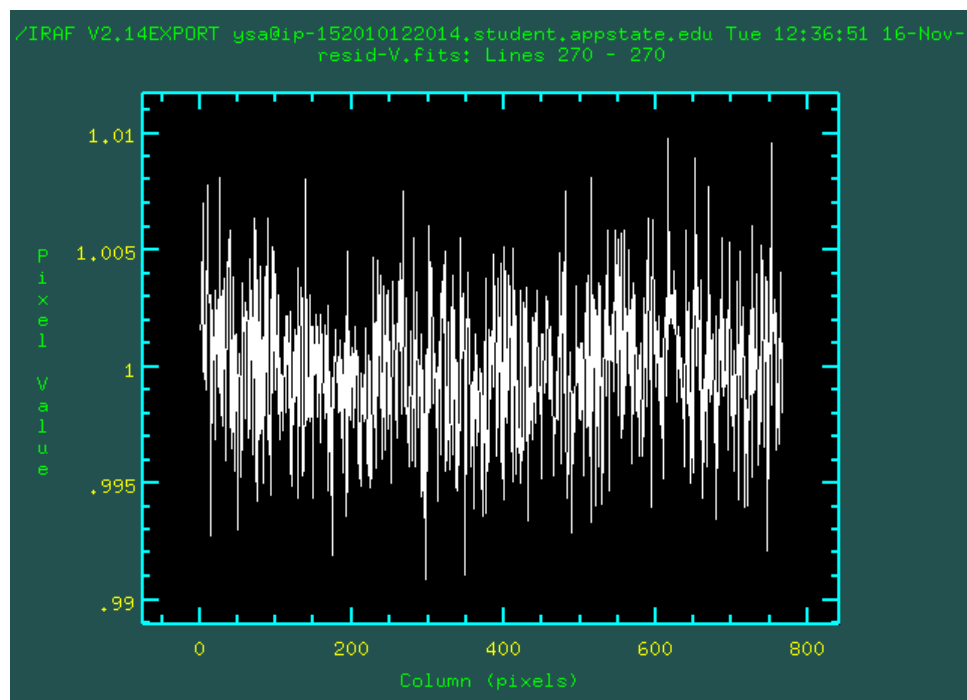


**Figure 4.2** Horizontal slice of the residual of the V-filter flat fields showing a difference of  $\sim 0.1\%$  across the chip.

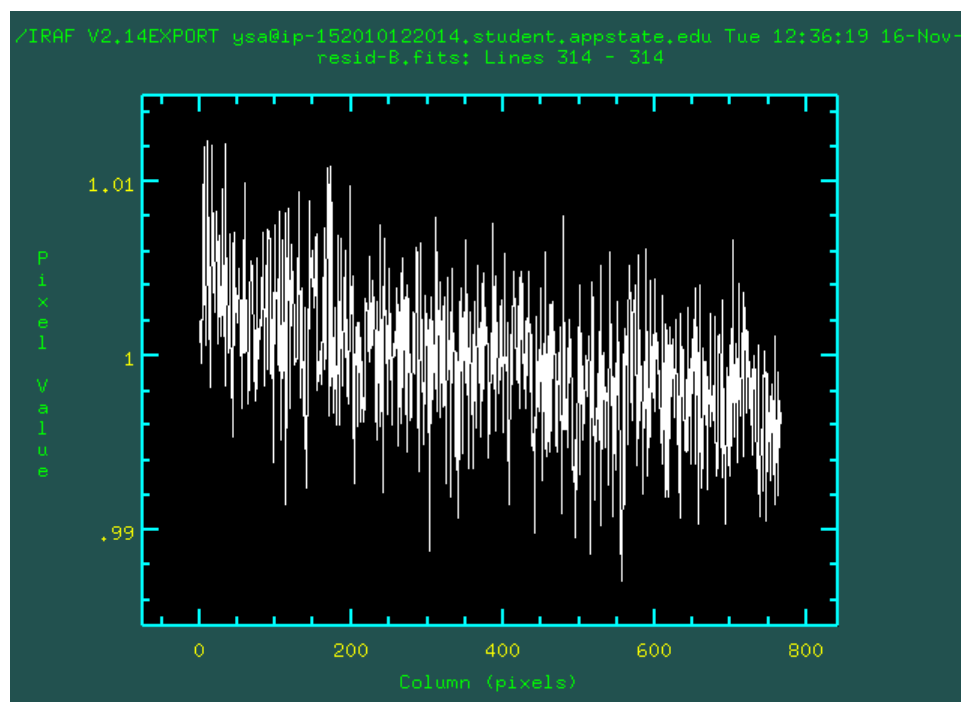


**Figure 4.3** Horizontal slice of the residual of the B-filter flat fields showing a difference of  $\sim 0.5\%$  across the chip.

# Chapter 5

## Reduction and Photometry

### Pipeline

The Reduction and Photometry Pipeline that I wrote for this project uses the Image Reduction and Analysis Facility (IRAF)<sup>1</sup>. It utilizes the IRAF scripting language “cl”, which allows for any package or command used from the IRAF command line to be called in an automated fashion. The script, called `imageproc_final.cl`, which is shown in Appendix A, follows the normal reduction of astronomy images with flat fielding and dark and bias subtracting.

Before any of the data reduction is done, the script takes the flats and darks for the night and combines them to form a master flat for each filter and master darks. Since the setup of the images between the PROMPT Array and the DSO telescopes is different, the program asks the user which observatory was used in order to create these master calibration images. These master calibration images are then applied

---

<sup>1</sup>IRAF is distributed by the National Optical Astronomy Observatory, which is operated by the Association of Universities for Research in Astronomy, Inc., under cooperative agreement with the National Science Foundation.

to the object images to create the reduced images. After the reduction is done, it outputs, for each filter, a combined image of all of the images in the series. This is done because the combined image has a higher signal to noise ratio than a single image.

The user can then use the `Imexamine` task in IRAF to determine the full width at half maximum (FWHM) and sigma of the point spread function of the stars in the image. Those values are then entered into the data parameter file `datapars`. This parameter file is needed to use the IRAF tasks `DAOfind` and `Phot`.

The user then uses a second script called `photometry.c1`, shown in Appendix B, which uses the IRAF task `DAOFind` to find every star in the field. These coordinates are then plugged into the IRAF task `Phot`. That task carries out aperture photometry on each star in the field that is present in the coordinate list generated by the task `DAOFind`.

# Chapter 6

## Results

Using the IRAF reduction and photometry pipeline that I wrote and discussed in Chapter 5, I created light curves for the Johnson-Cousins B, V, and I filters for two different YSAs. These YSAs are HD 189733 and HD 209393. These YSAs were chosen because they each had a number of stars in the field with magnitudes similar to that of the star in question. This is important because high-precision photometry requires stars with similar magnitudes to that of the target star. These light curves include data from JD 2455464 to JD 2455500, or a little over a month of data.

### 6.1 HD 189733

The light curve for HD 189733, shown in Figure 6.1, is based on multiple sets of exposures on several of the nights. The photometry is differential with respect to a single comparison star, as shown in Figure 6.2. On some of the nights, multiple data sets were obtained for a single star. The agreement between those single-night data are generally quite good ( $\pm 0.01$  mag) and generally smaller than the night-to-night variations observed.

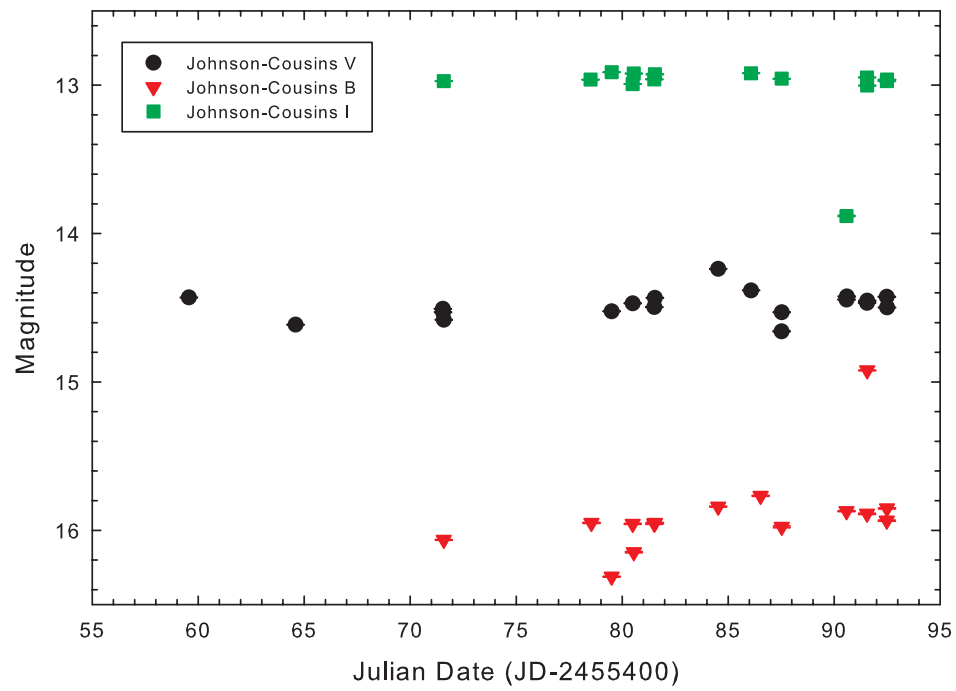


**Figure 6.1** Johnson-Cousins B, V, and I filter light curves of HD 189733.

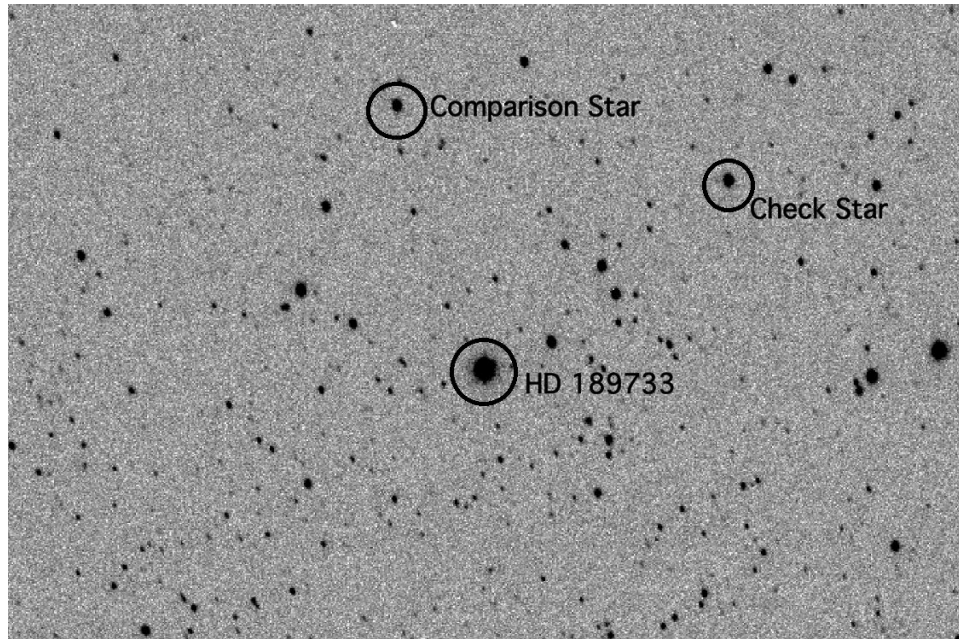


**Figure 6.2** Finder chart for HD 189733 showing the comparison stars used.

HD 189733 shows some apparently periodic variations, but more data are required before we can attribute these variations to rotation. This periodic effect is apparent in more than just one filter.

One effect that was prevalent in the data reduction is the effect of clouds on the photometry. While looking at the individual images the clouds were hard to detect, but when looking at the reduced and combined data, there were sets that showed the stars blurred by the passage of clouds as shown in Figure 6.3. Also, this was evident in a few sets where the stars drifted two or three stellar diameters over the course of a set of exposures as shown in Figure 6.4. This can happen when clouds pass over the guide star and the observer must resort to manual tracking, which is almost impossible to do due to the high degree of accuracy needed to combine a series of images. Also, it was noticed that the stability of the focus on the original piggyback

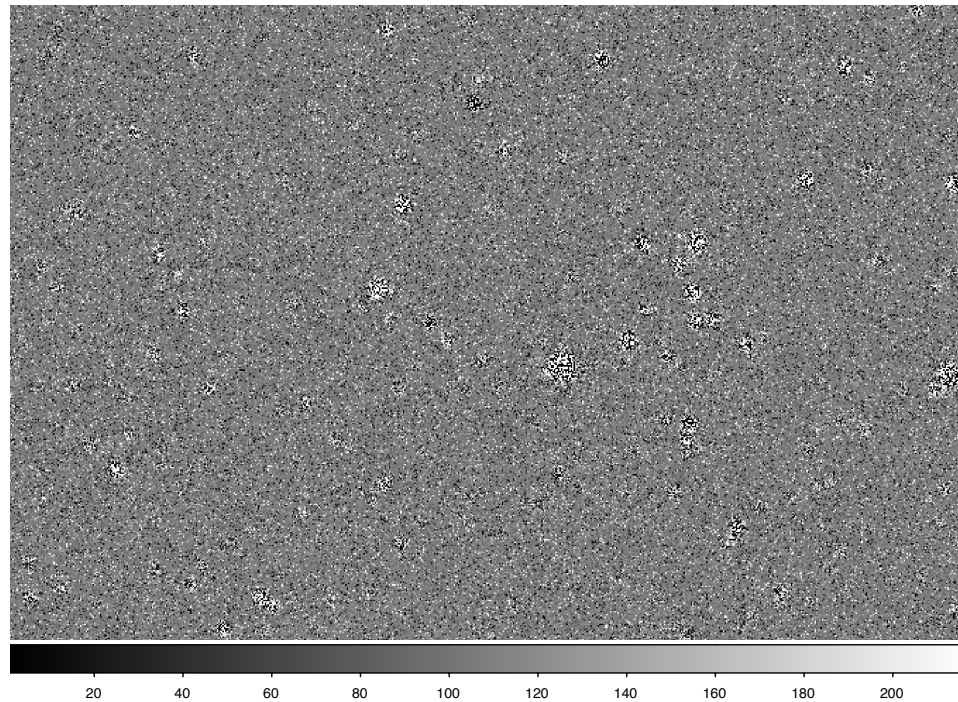


**Figure 6.3** A sample image of the effect of clouds on the combined images where the stars are very blurred.

telescope can cause some issues in the images when they are combined, as shown in Figure 6.5.

### 6.1.1 Multiple Comparison Star Test

Since for HD 189733 we have several nights with multiple sets of data, we were able to try using multiple comparison stars to reduce the scatter in magnitudes that was noted in the previous section about HD 189733. The actual measurements for HD 189733 and the three comparison stars are listed in Table 6.1.

From these data, an average of the V magnitudes for the comparison stars was calculated for both sets of data. For series 1, this average is 14.037, and for series 2, it is 14.044. These values were then subtracted from the HD 189733 V magnitude.

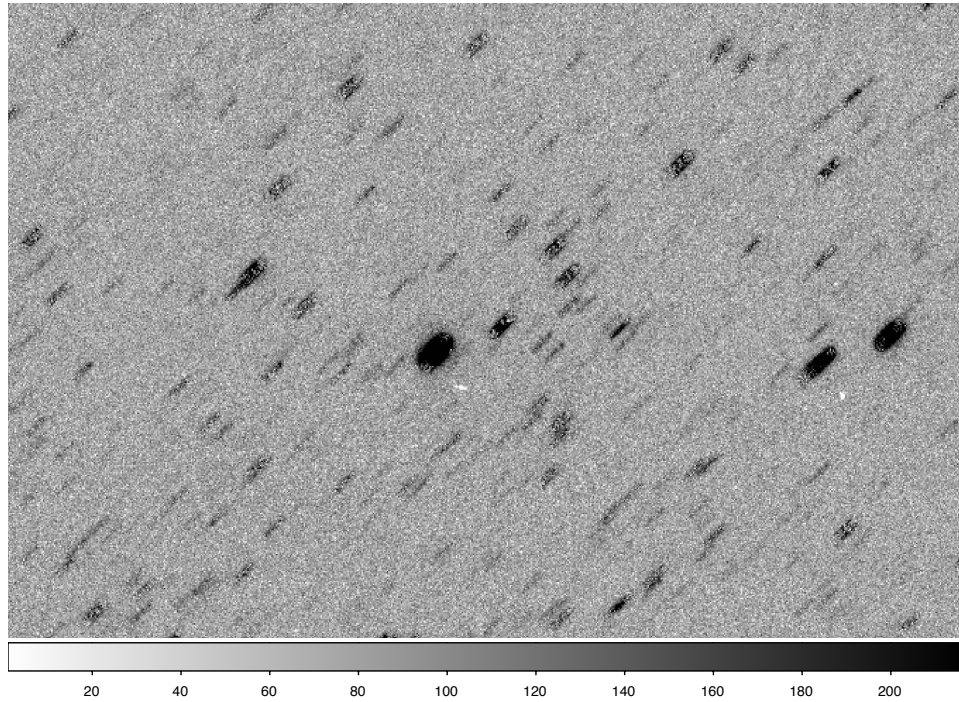


**Figure 6.4** A sample image showing drift of the stars.

For series 1, this difference is -2.449, and for series 2, it is -2.453. These two difference magnitudes agree to within 0.004 mag. This is a significant result because it bodes well for milli-magnitude precision, which will help eliminate the scatter in the data for HD 189733 obtained on the same night but in different sets.

With the replacement of the old 5-inch piggyback with the new 6-inch piggyback and its corresponding camera, the use of the multiple comparison star technique will yield higher precision photometric results. This is the case because the new setup will allow for a larger number of comparison stars.

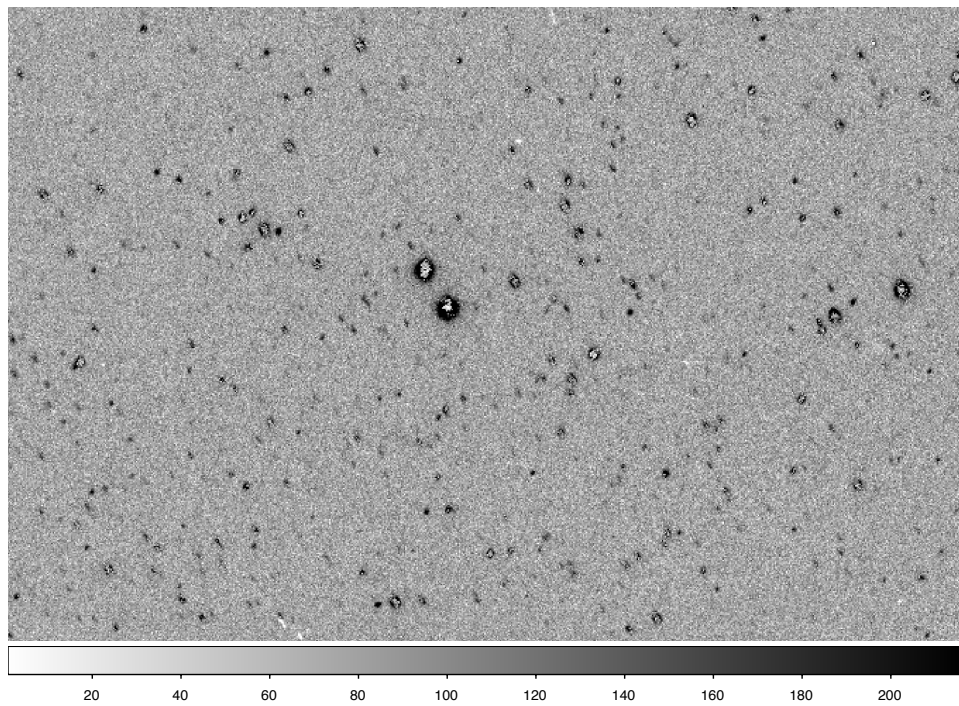


**Figure 6.5** A sample image of the effect of focus shift over a series of images has on the combined image.

<b>HD 189733 V Series 1</b>				
Star	X	Y	V mag	err
1	378	249	11.588	0.003
2	551	382	14.727	0.033
3	248	304	14.559	0.028
4	700	262	12.826	0.007
			14.037 = av(2,3,4)	
			<b>mag(1) - av(2,3,4) = -2.449</b>	
<b>HD 189733 V Series 2</b>				
Star	X	Y	V mag	err
1	372	243	11.591	0.003
2	545	376	14.715	0.029
3	242	299	14.573	0.026
4	694	256	12.843	0.007
			14.044 = av(2,3,4)	
			<b>mag(1) - av(2,3,4) = -2.453</b>	
<b>Difference = -2.449 - (-2.453) = 0.004</b>				

**Table 6.1** This table includes the results of the multiple comparison star test on HD 189733. In this table, star 1 is HD 189733 and stars 2, 3, and 4 are the comparison stars.

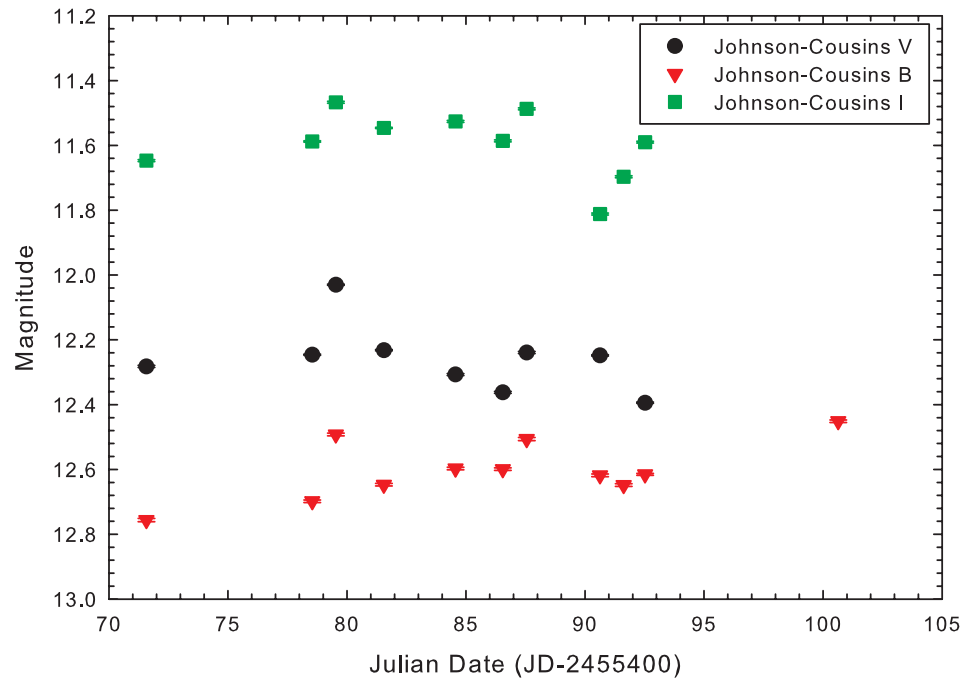


**Figure 6.6** Johnson-Cousins B, V, and I filter light curves of HD 209393.

## 6.2 HD 209393

The light curve for HD 209393, shown in Figure 6.6, uses one comparison star, identified in Figure 6.7. Some interesting effects are seen. There seems to be some slope in the magnitudes over the period in question. The interesting thing is that the B-filter light curve has a slightly negative slope (getting dimmer), while V and I show slightly positive slopes. This suggests either HD 209393 is becoming redder or the comparison star is becoming bluer. Clearly this will need to be investigated further with more data in the future.

In the case of HD 209393, there are no single-night multiple sets of exposures. This limits the ability to determine if there are any discrepancies in the data which would be indicated by significant variations in a single night.

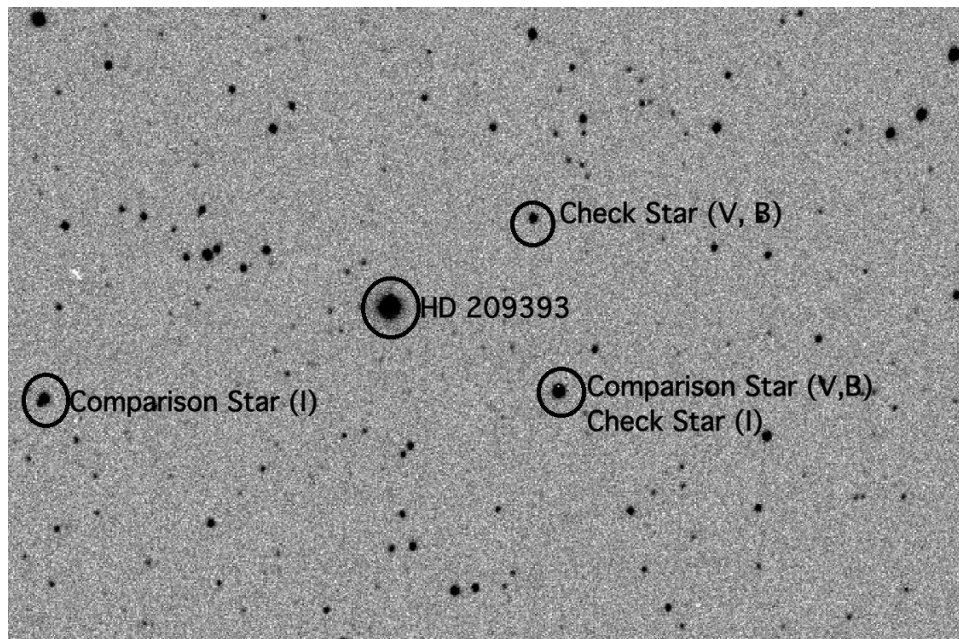


**Figure 6.7** Finder chart for HD 209393 showing the comparison stars used.

# Chapter 7

## Conclusions

Unfortunately, the photometric results from the PROMPT telescope array were disappointing. This is a result of apparently irreducible systematic and random errors on the 4% level, which is above the milli-magnitude precision required for this project. The sources of these inconsistencies are still not fully understood, but may be connected with stray light from the open-tube telescope and clamshell domes. Also, the small field of view ( $10'$ ) of the Skynet scopes did not provide optimal comparison and check stars. The expansion of the photometric study with the piggyback scope and robotic mount has significantly improved the photometry. The luminescent panel flip-flats are providing photometry stable to better than 1%. The stability and accuracy of the flats obtained from the flip-flats gives significant evidence that the flip-flat technique and technology can be utilized and is a viable replacement for sky dusk and twilight flats.

This research has shown some promising results with some apparently periodic variations visible in the light curves. Also, the milli-magnitude precision that is obtainable through the multiple comparison star techniques combined with the stability

of the luminescent panel flip-flats is very promising. These results imply that the precision and accuracy required for the YSA project are achievable.

The research has also shown that there are still a few things to consider. One of the things that came up while looking at the data is whether it is worthwhile to try and observe on partially cloudy nights. While under normal photometric situations occasional clouds are not an issue because the clouded images can be easily removed, in our case where we are combining a set of images into a single image, this can be problematic since it is harder to eliminate clouded images. In addition, we experienced some pointing issues with the 32-inch piggyback telescope, although it appears this is the result of clouds causing the loss of the guide star.

The techniques and procedures I have established over the course of this project will be utilized over the next 10 or so years in the long-term project that Dr. Gray is heading. The instrumentation work that has been done during this project, including the installation of the piggyback telescope on the DSO 32-inch telescope and the development of the robotic telescope, will also be utilized in the long term project. My research which used some data from the original telescopes led to the replacement of the original instruments with ones that allow for a wider field of view. These improvements combined with the use of multiple comparison stars will allow for high-precision photometry at the milli-magnitude level required to see stellar activity cycles and flares.

# Bibliography

Wilson, O.C. 1978, ApJ, 226, 379

Baliunas, S.L. et al. 1995, ApJ, 438, 269

Hempelmann A., Schmitt, J., Baliunas S.L., & Donahue, R.A. 2003, AA, 406, 39

Favata, F., Micela, G., Baliunas, S.L., Schmitt, J.H.M.M., Gudel, M., Harnden Jr.,  
F.R., Sciortino, S., & Stern, R.A. 2004, AA, 418, 13

Gaidos, E.J., Ganzalez, G., Gudel, M., Heap, S.R., & Henry, G.W. 2001, “Young  
Stars Near Earth: Progress and Prosepects”, 244, 81

Lockwood, G.W., Skiff, B.A., Henry, G.W., Henry, S., Radick, R.R., Baliunas, S.L.,  
Donahue, R.A., & Soon, W. 2007, ApJS, 171, 260

Soderblom, D.R. 1982, ApJ, 262, 239

Soderblom, D.R. 1983, ApJS, 53, 1

Reichart, D.E., Ivarsen, K.M., Haislip, J.B., Nysewander, M.C., & LaCluyze, A.P.  
2006, Nuvo Cimeto C, 28, 787

Hall, J., Henry, G.W., Lockwood, G.W., Skiff, B.A., & Saar, S.H. AJ, 138, 312

Guinan, E.F., & Engle, S.G. 2009, International Astronomical Union, IAU Symposium, 258, 395

# Appendix A

## IRAF imageproc\_final.cl code

```
list = ""
imdelete BIAS
imdelete DARK
imdelete FLAT
imdelete FLATDARK
imdelete Solar_analogs/temp/*
imdelete Solar_analogs/biastemp/*
delete Biasfiles.lis
delete Darkfiles.lis
delete Flatfiles.lis
delete Darkflat.lis
delete rawfiles.lis
delete filenam.lis
delete darknam.lis
delete nam.lis
delete imgfiles.lis
delete HDcomb.imh.coo
delete HDcomb.fits
delete HDcomb.mag

real t
real tim
real expd
real scale
real exps
int junk
int obsv
int comb
string c=""
```

```
string filter
string nam=""
string num=""
string filnam=""
string resfilt=""
string s4=""
string s5=""
string s6=""

copy ("Solar_analogs/Images/HD*", "Solar_analogs/Images/raw/")

files Solar_analogs/Images/raw/HD* >rawfiles.lis
list=""
list="rawfiles.lis"

i=1
while(fscan(list,s4) !=EOF)
{
if(i!=1)
{
imdelete (s4)
};
i=i+1
}

files Solar_analogs/Images/raw/HD* >filenam.lis
list=""
list="filenam.lis"
while(fscan(list,s5)!=EOF)
{
imgets (s5, "FILTER")
resfilt=imgets.value
imgets(s5, "EXPOSURE")
exps=real(imgets.value)
filnam=substr(s5,41,57);
}

copy ("Solar_analogs/Darks/*", "Solar_analogs/temp/")

files Solar_analogs/temp/* >darknam.lis
list=""
```

```
list="darknam.lis"

i=1
while(fscan(list,s6) !=EOF)
{
if(i!=1)
{
imdelete (s6)
};
i=i+1
}

files Solar_analogs/temp/* >nam.lis
list=""
list="nam.lis"

while(fscan(list,s2) !=EOF)
{
nam=substr(s2,40,67);
}

files Solar_analogs/Darks/DARK* >Biasfiles.lis
list = "Biasfiles.lis"

c="1"
i=1
while(fscan(list,s1) != EOF)
{
imgets(s1, "EXPOSURE")
tim = real(imgets.value)
if(tim==0)
{
if(i<10)
{
num="__00"
};
if(i>=10 && i<100)
{
num="__0"
};
if(i>100)
```

```
{
num="__"
};
copy ("Solar_analogs/Darks/"+nam+num+c+".fits", "Solar_analogs/Darks/biastemp/")
};
i=1+i
c=i
}

printf ("\nEnter 1 for Prompt or 2 for dso?\n")

if(obsv==1)
{
printf("%d\n",obsv)
imcombine Solar_analogs/biastemp/* BIAS combine=average
files Solar_analogs/Darks/DARK* >Darkfiles.lis
list = ""
list = "Darkfiles.lis"
c=""
c="1"
i=1
while( fscan(list,s1) != EOF)
{
imgets(s1,"EXPOSURE")
tim = real(imgets.value)
if(tim==exps)
{
if(i<10)
{
num="__00"
};
if(i>=10 && i<100)
{
num="__0"
};
if(i>100)
{
num="__"
};
copy ("Solar_analogs/Darks/"+nam+num+c+".fits", "Solar_analogs/temp/")
};
```

```
if(tim!=exps)
{
if(tim==2.5)
{
if(i<10)
{
num="__00"
};
if(i>=10 && i<100)
{
num="__0"
};
if(i>100)
{
num="__"
};
copy ("Solar_analogs/Darks/"+nam+num+c+".fits", "Solar_analogs/temp/")
imarith("Solar_analogs/Darks/"+nam+num+c+".fits", "/",2.5,"Solar_
analogs/Darks/"+nam+num+c+".fits")
imarith("Solar_analogs/Darks/"+nam+num+c+".fits", "*",exps,"Solar_
analogs/Darks/"+nam+num+c+".fits")
};
};
i=1+i
c=i
}

delete Darkfiles.lis
files Solar_analogs/temp/* > Darkfiles.lis
list = ""
list = "Darkfiles.lis"

while( fscan(list,s1) !=EOF)
{
imarith(s1, "-", "BIAS",s1)
}
imcombine Solar_analogs/temp/* DARK combine=average

delete Darkflat.lis
files Solar_analogs/Darks/* >Darkflat.lis
```

```
list = ""
list = "Darkflat.lis"
c=""
c="1"
i=1
while(fscan(list,s2) !=EOF)
    {
    imgets(s2,param="EXPOSURE")
    expd = real(imgets.value)
    if(expd==2.5)
    {
    if(i<10)
    {
    num="__00"
    };
    if(i>=10 && i<100)
    {
    num="__0"
    };
    if(i>100)
    {
    num="_"
    };
    copy ("Solar_analogs/Darks/"+nam+num+c+".fits", "Solar_analogs/ftemp/")

    imarith("Solar_analogs/ftemp/"+nam+num+c+".fits", "/",2.5,"Solar_analogs/
ftemp/"+nam+num+c+".fits")
    };
    i=1+i
    c=i
    }
    }
imcombine Solar_analogs/ftemp/* FLATDARK combine=average
if(obsv==2)
{
imcombine Solar_analogs/Darks/* DARK combine=average
}
files Solar_analogs/Flats/F* >Flatfiles.lis
list = ""
list = "Flatfiles.lis"
c=""
```

```
c="1"
i=1
if(obsv==1)
{
while(fscan(list,s3) !=EOF)
{
imgets(s3,"FILTER")
filter=imgets.value
if(filter !=resfilt)
{
imdelete (s3)
};
if(filter==resfilt)
{
imgets(s3,"EXPOSURE")
{
tim = real(imgets.value)
};
t=tim/expd
imarith("FLATDARK", "*",t,"FDtemp")
imarith(s3, "-", "FDtemp",s3)
imstat(s3,fields="midpt",format-) | scan(y)
z=1/y
imarith(s3, "*",z,s3)
imstat(s3,fields="midpt",format-) | scan(y)
print(y)
imdelete FDtemp
}
i=1+i
c=i
};
}
else
{
while(fscan(list,s3)!=EOF)
{
imarith(s3,"-","FLATDARK",s3)
imstat(s3,fields="midpt",format-) | scan(y)
z=1/y
imarith(s3, "*",z,s3)
imstat(s3,fields="midpt",format-) | scan(y)
```

```
print(y)
}
}
imcombine Solar_analogs/Flats/* FLAT combine=average
imstat("FLAT.fits",fields="midpt",format-)|scan(y)
z=1/y
imarith("FLAT.fits","*",z,"FLAT.fits")
imstat("FLAT.fits",fields="midpt",format-)|scan(y)
print(y)

files Solar_analogs/Images/HD* >imgfiles.lis

list=""
list="imgfiles.lis"

s1=""
while( fscan(list,s1) !=EOF)
{
imarith(s1, "-", "DARK",s1)
if(obsv==1)imarith(s1, "-", "BIAS",s1)
imarith(s1, "/", "FLAT",s1)
}

imcombine Solar_analogs/Images/HD* HDcomb reject=avsigclip
display HDcomb.fits erase=yes zscale= no contrast=0.5 nsample=1000

del Solar_analogs/Darks/*
del Solar_analogs/Images/HD*
del Solar_analogs/Images/raw/*
del Solar_analogs/Flats/*
del Solar_analogs/ftemp/*
del Solar_analogs/temp/*
```

# Appendix B

## IRAF photometry.cl code

```
noao  
digiphot  
apphot
```

```
daofind HDcomb.fits output="default" threshold=100 readnoise=17  
interactive=no verify=no
```

```
phot HDcomb.fits coords="default" output="default" interact=no verify=no
```